Journal of Sound and Vibration 330 (2011) 1074–1090

Contents lists available at ScienceDirect

Journal of Sound and Vibration

journal homepage: www.elsevier.com/locate/jsvi

# Non-ambiguous recovery of Biot poroelastic parameters of cellular panels using ultrasonic waves

Erick Ogam [a,*], Z.E.A. Fellah [a], Naima Sebaa [b], J.-P. Groby [c]

[a] CNRS Laboratoire de Mécanique et d'Acoustique UPR7051, 31 chemin Joseph Aiguier, 13402 Marseille cedex 20, France
[b] Laboratorium voor Akoestiek en Thermische Fysica, Katholieke universiteit, Heverlee, Belgium
[c] Laboratoire d'Acoustique de l'Université du Maine, UMR 6613 CNRS/Université du Maine, Avenue Olivier Messiaen, 72085 Le Mans Cedex 09, France

ARTICLE INFO

*Article history:*
Received 23 August 2009
Received in revised form
4 September 2010
Accepted 28 September 2010
Handling Editor: R.E. Musafir
Available online 14 October 2010

ABSTRACT

The inverse problem of the recovery of the poroelastic parameters of open-cell soft plastic foam panels is solved by employing transmitted ultrasonic waves (USW) and the Biot–Johnson–Koplik–Champoux–Allard (BJKCA) model. It is shown by constructing the objective functional given by the total square of the difference between predictions from the BJKCA interaction model and experimental data obtained with transmitted USW that the inverse problem is ill-posed, since the functional exhibits several local minima and maxima. In order to solve this problem, which is beyond the capability of most off-the-shelf iterative nonlinear least squares optimization algorithms (such as the Levenberg Marquadt or Nelder–Mead simplex methods), simple strategies are developed. The recovered acoustic parameters are compared with those obtained using simpler interaction models and a method employing asymptotic phase velocity of the transmitted USW. The retrieved elastic moduli are validated by solving an inverse vibration spectroscopy problem with data obtained from beam-like specimens cut from the panels using an equivalent solid elastodynamic model as estimator. The phase velocities are reconstructed using computed, measured resonance frequencies and a time–frequency decomposition of transient waves induced in the beam specimen. These confirm that the elastic parameters recovered using vibration are valid over the frequency range of study.



## 1. Introduction

The motivation of this study is the need for simple and efficient methods for the characterization of the microstructure and mechanical behavior of cellular materials. The aim of the investigation is the resolution of the *inverse problem* of retrieval of poroelastic parameters of air-saturated cellular materials in the form of panels from transmitted ultrasonic wave data, with an emphasis on finding the correct minimum from the cost (objective) function.

The poroelastic properties of cellular materials are complex, dependent upon the material, the saturating fluid, as well as the microstructural arrangement. Details in constituent cells of foams relating to the micro-mechanics governing the deformation and failure mechanisms which determine the overall foam responses have yet to be elicited [1]. Many studies involving the detailed analysis of the microstructural features such as cell size, geometry of constituent cells and the struts that define the cell edges, as well as their stiffness and tensile strength have been undertaken for plastic foams and a good

* Corresponding author. Tel.: +33 4 91 16 44 82; fax: +33 4 91 16 42 70.
*E-mail address:* ogam@lma.cnrs-mrs.fr (E. Ogam).

0022-460X/$ - see front matter © 2010 Elsevier Ltd. All rights reserved.
doi:10.1016/j.jsv.2010.09.032

number can be found in [2]. In these studies, the nature of cell morphology, anisotropy and deformation are identified through microscopy (optical or scanning electron microscope) or micro-computed X-ray tomography. The associated micro-mechanics is often analyzed using Kelvin cell models [3–6] which predicts well the shape of the compressive stress–strain curve. In acoustics, microstructural configurations have been used to study how the volume averaged properties of the thermal and velocity fields governing the propagation and dissipation of acoustic waves relate to microscopic details of the local geometry parameters [7].

The investigation focuses on the development of the direct and inverse problem of retrieval of the macroscopic structural (porosity, viscous and thermal characteristic lengths, tortuosity [8,9]) and macroscopic mechanical (Young's modulus, Poisson ratio and density) properties of poroelastic, soft open-cell foam panels. Ultrasonic wave propagation in the poroelastic panels is modeled using a modified Biot's theory where the parameters have physical interpretation closely related to the pore structure at the microscale. This model for air-saturated cellular material is detailed in Section 2 and the method for solving the inverse problem in Section 3.

The quality of the reconstruction of material parameters often varies with the accuracy of the data on the one hand, and the accuracy of the interaction model employed in the inversion scheme on the other hand [10]. It is shown that even though the employed method uses an estimator (mathematical entity used to account for the wave field transmitted by a test target) that is exact for a poroelastic panel problem, it leads to an infinite number of solutions for the inverse problem of the reconstructed parameters when the probe radiation is a band-limited plane wave [11]. This is a problem because of the difficulty in the choice of the right solution from several minima of the cost function.

A consequence of ill-posedness is that arbitrarily small changes in the data may lead to arbitrarily large variations in the solution of the inverse problem. Since data errors are inevitable, stabilizing procedures termed regularization are often employed to successfully deal with ill-posedness [12]. A method to handle the ill-posed problem using the cost function is proposed in Section 4. In previous studies [13,14], cost functions have been plotted within a certain range of expected solution values, in a manner similar to that practiced in optimization problems where the initial value for the algorithm is often chosen in the neighborhood of the solution. In this study a wide range of the solution space is examined to capture a large number of minima.

The ultrasonic wave transmission experimental procedure used herein is developed in Section 5. The detailed description of the panels is given in Section 5.1.

In Section 6 the acoustic parameters recovered with the present model are validated using the model of equivalent fluid (MEF), the reference method for the characterization of soft open-cell foams, in which the porous material is replaced on a macroscopic scale by an equivalent fluid [15–19]. A second method is used to deduce the tortuosity from the asymptote of the calculated phase velocities in the high-frequency region using transmitted USW as outlined in [20].

The second part of the investigation concerns the inverse problem of the recovery of elastic parameters from real vibrational data for the validation of those previously recovered using transmitted ultrasonic wave data. This is done using simplified vibration spectroscopy elastodynamic model of a sub-specimen of the aforementioned cellular panel structures in the form of long, thin cross-sectioned beams.

The multimodal and dispersive nature of wave propagation in beams (many modes can propagate simultaneously with velocities depending on frequency) will influence the vibration spectroscopy data used in the inverse problem. The resolution of the direct vibration spectroscopy problem is done by solving two eigenvalue problems. The first is implemented using a 3D finite element model scheme for the lower frequency modes. The second involves the resolution of an eigenvalue problem for the Timoshenko beam model equation in order to better capture the higher frequency flexural modes. The equation is solved using a fourth-order finite difference scheme.

Since the beams are porous, employing the simpler elastodynamic models to recover elastic parameters requires that the dispersion observed using phase velocities in the frequency band of interest, be accounted for in the models. The dispersion accounted for by the elastodynamic models are those due to shear and rotary inertia and Poisson effect [21,22]. The elastic parameters of the beams are validated qualitatively using known asymptotic regions of the phase velocity curves. The method for attaining this objective using time frequency analysis on acquired data pertaining to the transient waves propagating in the beams is also detailed herein.

The results are given in Section 8.

## 2. The forward problem for the transmission of an acoustic wave by a porous plate-like panel

The forward transmission problem (notably for simulating measured data) is formulated as follows. Given: (i) the geometry of the transmitting porous plate (panel) body and its composition (material properties); (ii) the material properties of the host medium; (iii) the incident wavefield, determine: the field transmitted through the body at arbitrary points of space.

Biot theory describes the equations of motion for each phase (i.e., the solid frame and the fluid) based on energy considerations that include the inertial, potential, and viscous coupling between the two phases. The macroscopic average displacement vectors $\mathbf{u}$ and $\mathbf{U}$ for, respectively, the solid and the fluid in the fluid saturated porous medium, are given by

$$\tilde{\rho}_{11}\frac{\partial^2\mathbf{u}}{\partial t^2}+\tilde{\rho}_{12}\frac{\partial^2\mathbf{U}}{\partial t^2}=P\nabla(\nabla\cdot\mathbf{u})+Q\nabla(\nabla\cdot\mathbf{U})-N\nabla\wedge(\nabla\wedge\mathbf{u}), \tag{1}$$

$$\tilde{\rho}_{12}\frac{\partial^2\mathbf{u}}{\partial t^2}+\tilde{\rho}_{22}\frac{\partial^2\mathbf{U}}{\partial t^2}=Q\nabla(\nabla\cdot\mathbf{u})+R\nabla(\nabla\cdot\mathbf{U}), \tag{2}$$

where $P$, $Q$ and $R$ are the macroscopic Biot elastic constants [8,23] which are related, via Gedanken experiments, to other, measurable quantities, namely the porosity, bulk modulus of the pore fluid ($K_f$), bulk modulus of the elastic solid ($K_s$), bulk modulus of the skeleton ($K_b$), the shear modulus of the skeleton ($N$), elastic parameters : Young's modulus (YM) and Poisson ratio of the solid ($E_s$ and $\nu_s$, respectively) and of the skeleton ($E_b$ and $\nu_b$). The solid and skeleton frame compressibility moduli are given by

$$K_s=\frac{E_s}{3(1-2\nu_s)},\quad K_b=\frac{E_b}{3(1-2\nu_b)},\quad N=\frac{E_b}{2(1+\nu_b)}. \tag{3}$$

In order to extend this theory to a high frequency range, a correction factor, which modifies the fluid density through a tortuosity factor $\alpha$ in the form: $\rho_f\rightarrow\rho_f\alpha$, was introduced in [17]. Consequently the evaluation of the effective density of the fluid in the pores is no longer restricted to materials with cylindrical pores as in the original theory. Tortuosity represents the squared ratio of the mean path length through the porous frame to that of the direct path. It express the viscous exchanges between the fluid and the structure which play an important role in damping the acoustic waves in porous medium. When the frequency dependent effects are taken into account, it is called the dynamic tortuosity $\alpha(\omega)$ [17]:

$$\alpha(\omega)=\alpha_\infty\left(1+\frac{\sigma\phi}{\mathrm{j}\omega\alpha_\infty\rho_f}\sqrt{1+\mathrm{j}\omega\frac{4\alpha_\infty^2\rho_f\eta}{\sigma^2\Lambda^2\phi^2}}\right), \tag{4}$$

with $\mathrm{j}=\sqrt{-1}$, $\omega$ is the angular frequency, the resistivity $\sigma=\eta/k_0$, $\eta$ is the fluid viscosity, $k_0$ is the viscous permeability, $\phi$ is the porosity ($\phi=1-\rho_b/\rho_s$, for open pores only, where $\rho_b$ and $\rho_s$ are the densities of the skeleton and the solid, respectively), $\alpha_\infty$ is the tortuosity, $\Lambda$ is the viscous characteristic length (related to the size of the inter-connections between two pores).

The Biot coefficients are given by

$$\tilde{\rho}_{mn}=\rho_{mn}+(-1)^{m+n}\frac{b}{\mathrm{j}\omega}, \tag{5}$$

where $b$ is the drag coefficient, $\rho_{11}$ and $\rho_{22}$ are density parameters for the solid, $\rho_{12}$ is a density coupling parameter between the fluid and solid phases ($\rho_{11}+\rho_{12}=(1-\phi)\rho_s$, $\rho_{12}+\rho_{22}=\phi\rho_f$ and $\rho_{12}=-\phi\rho_f(\alpha_\infty-1)$).

When the pore fluid is light (e.g. gas), several modifications are needed in the Biot model equation. Thermal effects are added to the viscous relaxation phenomena associated with the dissipative properties of the porous solid. The ratios $K_b/K_s\ll1$ and $K_f/K_s\ll1$ and consequently the expressions of the constants $P$, $Q$ and $R$ are then given by

$$P=K_b+\frac{4}{3}N+\frac{(1-\phi)^2}{\phi}K_f^*,\quad Q=(1-\phi)K_f^*,\quad R=\phi K_f^*, \tag{6}$$

where the incompressibility modulus is a function of the compressibility $K_f$ and of the susceptibility $\beta(\omega)$ and is given by $K_f^*=K_f/\beta(\omega)$.

Thermal transfer between the air saturating the pores and the structure is due to the compression and dilatation of the former during the passage of the wave. This thermal transfer due to the interaction between the gas (in our case air) and the structure is modeled in the frequency domain by $\beta(\omega)$ [24]:

$$\beta(\omega)=\gamma-(\gamma-1)\left(1+\frac{\eta\phi}{\mathrm{j}\omega\rho_f k'_0 P_r}\sqrt{1+\mathrm{j}\frac{4\rho_f k'^2_0\omega P_r}{\eta\phi^2\Lambda'^2}}\right)^{-1}, \tag{7}$$

where $\gamma$ is the specific heat ratio, $k'_0$ the thermal permeability, $\Lambda'$ the thermal characteristic length and $P_r$ the Prandtl number. $K_f=\gamma P_0$ with $P_0$ the pressure of the saturating fluid.

In the high frequency regime ($\omega\rightarrow\infty$), the viscous skin thickness ($\delta=2\eta/\omega\rho_f$) is very thin near the radius of the pore $r$. The viscous effects are concentrated in a small volume near the surface of the frame and $\delta/r\ll1$, consequently the following asymptotic approximations are used:

$$\alpha(\omega)=\alpha_\infty\left(1+\frac{2}{\Lambda}\sqrt{\frac{\eta}{\mathrm{j}\omega\rho_f}}\right),\quad \beta(\omega)=1+\frac{2(\gamma-1)}{\Lambda'}\sqrt{\frac{\eta}{\mathrm{j}\omega\rho_f P_r}}, \tag{8}$$

where $\Lambda'$ is the thermal characteristic length (related to the size of the cell, the edge breadth of the ligament [7]) (Fig. 1). In this study $\Lambda'=3\Lambda$ (classically fixed from 2 to 3 for plastic foams [25]).

Finally, the coefficients of the Biot model with the corrections (in the frequency domain) are written:

$$\tilde{\rho}_{11}(\omega)=\rho_{11}+\frac{2\phi\alpha_\infty}{\Lambda}\sqrt{\frac{\eta\rho_f}{\mathrm{j}\omega}},$$

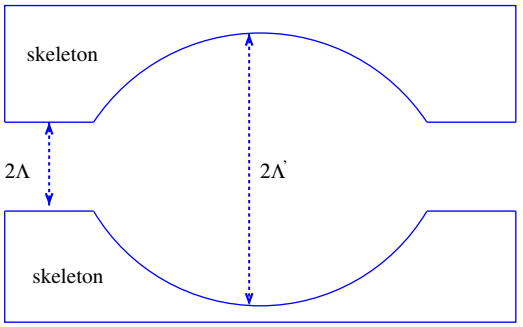


**Fig. 1.** Schematic representation of a pore. $\Lambda$ and $\Lambda'$ are the viscous and thermal characteristic lengths, respectively. They are related to the size of the inter-connection between two pores and the diameter of the pores, respectively.

$$\tilde{\rho}_{12}(\omega)=\rho_{12}-\frac{2\phi\alpha_\infty}{\Lambda}\sqrt{\frac{\eta\rho_f}{j\omega}},$$

$$\tilde{\rho}_{22}(\omega)=\rho_{22}+\frac{2\phi\alpha_\infty}{\Lambda}\sqrt{\frac{\eta\rho_f}{j\omega}}. \tag{9}$$

This modified Biot model is called henceforth BJKCA.

The displacement and pressure fields for the compressional waves are obtained by using the wave equations of the dilatational and rotational waves employing scalar and vector potentials, respectively. Since the acoustic wave impinges at normal incidence on the fluid-porous material interface, only longitudinal waves are excited. The displacement fields for the longitudinal vector components are

$$\mathbf{u}=\nabla\tilde{\Phi}_s,$$

$$\mathbf{U}=\nabla\tilde{\Phi}_f, \tag{10}$$

where $\Phi_s$ and $\Phi_f$ are the scalar potentials for the frame and air, respectively.

The analytical calculation, in the frequency domain of the transmission coefficient $\mathcal{T}(\omega)$, is done using these potentials, Eq. (1) and the boundary conditions [26].

The incident ($p_i$) and transmitted ($p_t$) pressure fields are related to the transmission scattering operator $\tilde{\mathcal{T}}(t)$ via the convolution in the time domain:

$$p_t(x,t)=\int_0^t\tilde{\mathcal{T}}(\tau)p_i\left(t-\tau-\frac{x-L}{c_0}\right)d\tau, \tag{11}$$

wherein $c_0$ is the speed of sound outside the porous panel and $L$ is the porous panel thickness.

The scattering operator $\tilde{\mathcal{T}}(t)$ is first computed numerically by the inverse Fourier transform of $\mathcal{T}(\omega)$ [14]. Its analytical expression is calculated in the same manner as that detailed in [26]. The convolution of $\tilde{\mathcal{T}}(t)$ with the incident signal (Eq. (11)) gives the transmitted signal in the time domain.

## 3. Solving the inverse problem of recovering the poroelastic parameters using transmitted USW

The general inverse transmission problem is formulated as follows. Given: (i) the incident wavefield, (ii) the material properties of the host medium (iii) the transmitted wavefield, reconstruct the poroelastic parameters of the transmitting porous panel (plate). The thickness of the panel is determined by measurement using vernier calipers. In the framework of the modified Biot theory (BJKCA), the propagation of ultrasonic waves in a air-saturated cellular panel is conditioned by the parameters listed in Table 2.

The inverse problem is that of the recovery of the parameters characterizing the microstructure of the cellular material from the measured incident ($p_i$) and transmitted ($p_t$) waves employing the BJKCA model. These parameters influence the load-capacity, elasticity, noise absorption and thermal insulation of the material. The transmitted wave was found to be sensitive to six parameters characteristic of the microstructure: $\Lambda$, $\phi$, $\alpha_\infty$, $E_b$, $\nu_b$ and $\rho_b$. They are recovered by minimizing the objective functional $\mathfrak{J}$ (the others are assumed to be known)

$$\mathfrak{J}(\Lambda,\alpha_\infty,\phi,\rho_b,E_b,\nu_b)=\sum_{p=1}^{L_s}\{p_{t_{\text{experiment}}}(t_p)-p_{t_{\text{model}}}(t_p,\Lambda,\alpha_\infty,\phi,\rho_b,E_b,\nu_b)\}^2, \tag{12}$$

whereby $L_s$ is the length of the temporal signals and $\Lambda'=3\Lambda$. The other parameters intervening in the BJKCA model require very specialized apparatus or equipment for their determination. Consequently, they are taken from tabulated data

(saturating fluid characteristics, Prandtl's number $P_r$, density $\rho_f$, fluid viscosity $\eta$, specific heat ratio $\gamma$ and pressure of the saturating fluid $P_0$ are taken as 0.71, 1.2 kg/m$^3$, 1.85e−5 Pa s, 1.4, 1.0e5 Pa, respectively).

The objective functional curves are given with respect to one of the six problem variables, the others being fixed at their computationally optimal values, i.e., as 2D plots.

## 4. Method for solving the ill-posed problem of recovering the poroelastic parameters from USW measurements

Cost functions (CF) often depicted seem to exhibit single minima, which are an indication of unique solutions. But in some cases, if the interval of variation of the parameters is enlarged, other minima may appear. Most optimization algorithms (e.g. Nelder Mead in [27]) may retrieve solutions that are not global depending on the initial values entered into the algorithm. In this study, the consequence of several minima in the CF is the ambiguity in retrieving the correct parameter values. The ambiguity can be removed in several ways, namely: (1) Using two panels of different thicknesses cut from the same homogeneous specimen. The drawback of this method is the possible damage of the specimen in the cutting process. (2) Employing data acquired from the acoustic interrogation of the panel at different angles of incidence, which requires a goniometer. (3) By changing the saturating fluid, for example replacing air with helium [28] or argon [29]. (4) Employing transducers with different central frequencies. The coinciding minima on the CF curves obtained for two different configurations are taken to be the true solutions.

The use of two transducers with different central frequencies is chosen with the true solutions being the coinciding minima (provided it is legitimate to suppose that the parameters do not vary significantly within the ranges of the two transducer frequency bands).

## 5. USW experimental procedures

### 5.1. Foam specimens

Open-cell foam panels made from melamine and polyurethane foams (PUF) [5] are employed. Melamine foam is one of the best sound absorbing materials. Melamine wedges have been employed as linings of the anechoic chamber of the CNRS LMA in Marseille [30]. The two soft PUF characterized in this study are green (GPUF) and yellow (YPUF) in color (color does not necessarily signal foams with the same properties). The YPUF and GPUF panels are both 1.0 cm thick while the melamine panel is 2.0 cm thick. The scanning electron microscope images obtained using a tabletop Microscope Hitachi TM1000 showing the pore arrangements of the melamine and GPUF panels employed in this study are depicted in Fig. 2. The rough estimate of the pore and pore inter-connections sizes, ligament length and edge breadth can be retrieved from these micrographs. The variation of pore size within each foam is often within a relatively narrow range [4,5]. Micrographs are also useful for validating models relating for instance the cell dimensions (length and cross-section radius) of the ligament and other dimensions (e.g. cell height) to parameters like the macroscopic mechanical properties, relative density (porosity), relative Young's modulus. These models have been reported in [4,7,31–33]. The anisotropy of the foams was not considered in the study.

The density of the specimens was calculated from their weights, measured on an electronic balance (Denver Instruments SI-4200), and volume. They are listed in Table 1.

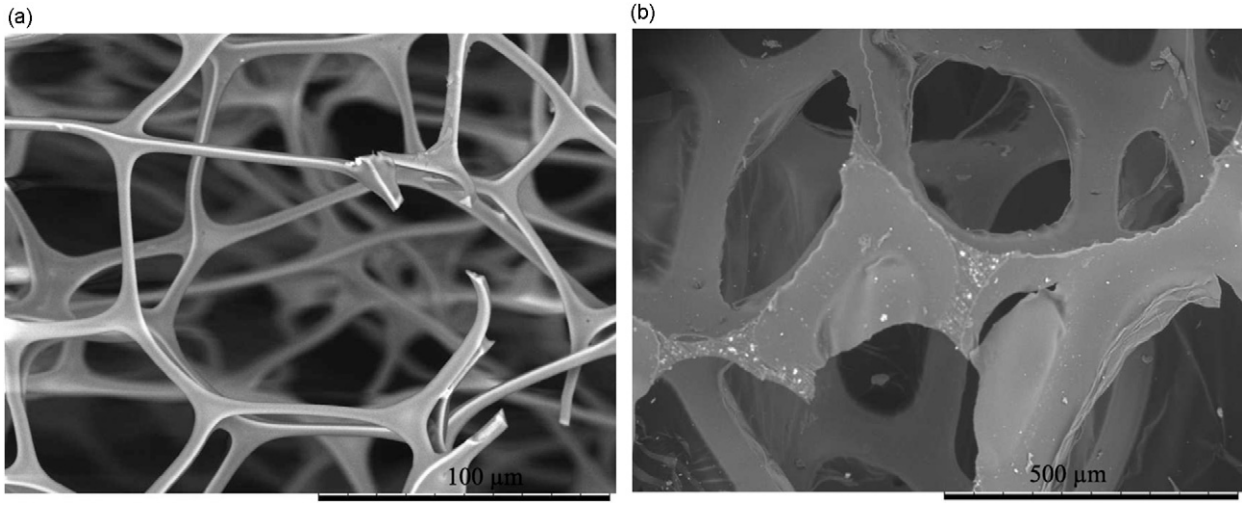


**Fig. 2.** SEM images of the pores of the characterized cellular panel samples. (a) Melamine foam. (b) Green polyurethane foam (GPUF).

**Table 1**
Measured geometric characteristics and density of the thin bar specimens cut from the foam panels.

| Foam specimen | Length (cm) | Cross section (cm × cm) | Measured density (kg/m$^3$) |
|---|---|---|---|
| Melamine | 29.8 | 1.5 × 1.5 | 8.0 |
| GPUF | | | 32.5 |
| YPUF | 32.5 | 1.0 × 1.5 | 27.8 |

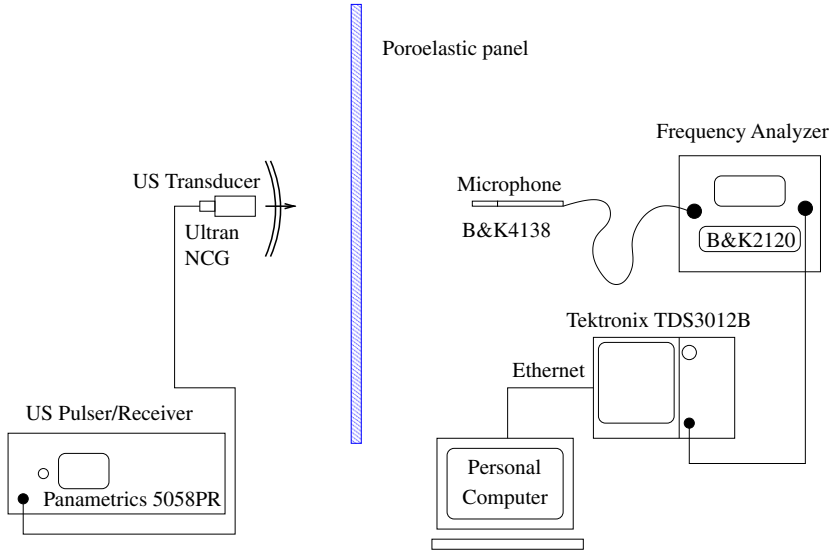


**Fig. 3.** The schematic of the measurement setup for acquiring the transmitted ultrasonic wave through a poroelastic panel immersed in air.

### 5.2. Ultrasonic measurements

Air-coupled ultrasonic probes with center frequencies at 50, 100 and 200 kHz (Ultran NCG50, NCG100, NCG200, respectively) connected to a Panametrics 5058-PR pulser are employed. The transmitted signal is captured using a B&K4138 microphone connected to a B&K2120 Analyzer for the 50 and 100 kHz probes. The schematic of the experimental setup is depicted in Fig. 3. For measurements at 200 kHz, two transducers (emitter and receiver) are connected to the Panametrics 5058-PR pulser. The transmitted signal in this case is captured using the air-coupled transducer and since the signal is highly attenuated, it is first amplified by low noise 40 dB preamplifier NF SA-200F3 and then by the 5058-PR pulser amplifier.

## 6. Validation of the acoustic parameters

The recovered acoustic parameters ($\Lambda,\phi,\alpha_\infty$) are validated using two methods.

### 6.1. Using the model of equivalent fluid

The structure of air-saturated cellular media is generally considered motionless in the absence of mechanical excitation and the waves to propagate only in the fluid at ultrasonic frequencies. The coupling of the acoustic energy from the air to the skeleton of the cells is negligible. This case is often described by the model of equivalent fluid [15,17–19]. This is an approximation of the Biot theory of poroelasticity [34,35]. The interactions between the fluid and the structure are accounted for in the two frequency response factors: the dynamic tortuosity of the medium and the dynamic compressibility of the saturating fluid as was detailed previously. The MEF is an interaction model whereby only the acoustic parameters can be recovered. The method of inversion appeals to the incident, reflected and transmitted waves as reported in [13]. The terms skeleton and foam are used as synonyms herein.

### 6.2. Using measured phase velocities in the high frequency regime

The tortuosity parameter of the open pore cellular panels is deduced directly from the measured phase velocities in the high frequency regime of the transmitted USW using the same test rig. The theoretical development is detailed in

Appendix A. Tortuosity $\alpha_\infty$ and viscous characteristic length $\Lambda$ can also be determined independently by solving an electrical conduction problem for a porous medium filled with a conducting fluid having an insulating solid phase [17]. $\alpha_\infty$ is obtained from the electrical resistivity measurement data as reported by Henry [36]. The most reliable method reported by this author requires the prior knowledge of the porosity of the sample.

## 7. Validation of USW mechanical parameters using vibration spectroscopy and transient wave measurement on thin beams

Vibration spectroscopy (VS) consists of setting a structure into vibration (linear or nonlinear) and then carrying out a spectroscopic examination of its vibrational response (resonance frequencies on the spectrogram). The vibration spectrogram is a function of the structure (material composition, geometry) and boundary conditions.

### *7.1. The forward VS problem for thin beam-like specimens cut from the panels*

The specimen is initially visualized as a linear, isotropic elastic solid 3D body of arbitrary shape, attached to its environment with a stress-free boundary condition, and submitted to a transient excitation. The microscopic irregularities and biphasic nature of the original porous medium are not explicitly taken into account; i.e., the medium is thought of as being homogenized on the scale of the micro-irregularities (but macro-irregularities can be accounted for by the 3D geometrical model). The procedure for computing the resonance frequencies using the elastodynamic model is established in Appendix B. This computation is easily carried out for the low frequency modes but requires finer finite element meshes for the high frequency ones thus resulting in longer computation times. In order to alleviate this problem, we chose a 1D formulation for the flexural modes, i.e., the specimen is considered to be a Timoshenko beam for which there exist two propagating modes. The method for calculating the resonance frequencies pertaining to the two modes using the finite difference method (FDM) is detailed in Appendix C. The elastodynamic interaction models employed (Timoshenko beam model and 3D FEM) account for the mode dispersions, consequence of the Poisson effect, shear deformation and rotary inertia.

### *7.2. Solving the inverse VS problem of recovering the elastic parameters of thin beam specimens*

The thin beam specimens are cut from the same panels as those characterized using USW. The macroscopic elastic moduli of the porous beams saturated with a light fluid, considered to be the same as those of the dry skeleton (Young's modulus $E_b$ and Poisson ratio $\nu_b$) are retrieved using the measured resonance frequencies of thin cellular beams in a setup in which they are suspended by nylon threads thus allowing the specimens to vibrate with stress-free boundary conditions. During the inversion process the beams are modeled using the previously mentioned equivalent 3D solid elastodynamic model (homogenous and isotropic). The details on the resolution of the inverse vibration spectroscopy (IVS) problem are given in Appendix D. Once the moduli are recovered, the forward problem is used to compute the resonance frequencies from these optimized values used to plot the phase velocities as explained in a later Section 7.2.2.

#### *7.2.1. Vibration spectroscopy measurements*

Thin bar specimens of melamine and YPUF with cross-sections 1.5 cm × 1.5 cm and 1.0 cm × 1.5 cm, respectively, are employed. The exciter is a piezoelectric transducer (PZT) bonded to one of the extremities of the thin bar specimen. It is driven using a power amplifier, Brüel and Kjaer B&K2706. The response is measured at the opposite end of the specimen using a sensor of the same type as the excitation PZT. The sensor output is connected to a low noise amplifier, Ciprian EO80 dB (Grenoble France).

In order to favor the longitudinal mode, the exciter is bonded using double sided scotch tape at the flat end of the thin bar while the sensor is bonded to the opposite extremity (Fig. 4). Flexural waves are favored by bonding the exciter and the sensor laterally to the specimen.

When the PZT sensor is bonded to a deforming vibrating surface, a mechanical deformation is induced in the polarized crystal (resulting from tension and twisting of the sensor) leading to the generation of an electric charge. Likewise, when the PZT crystal is submitted to a modulated electrical solicitation, it vibrates (and induces a stress wave). The light weight, small size and flat structure form of the PZT facilitates its mechanical fixation on structures, with negligible influence on the vibrational response as compared, for instance, to an accelerometer.

The exciter transducer (PZT) is driven using harmonic excitation at constant amplitude in discrete frequency steps using a digital signal processing Lock-in amplifier, Signal Recovery 7265 (Oak Ridge, USA), which also acquires the amplitude and phase of the response. The schematic is the same as that reported in [37].

#### *7.2.2. Method for plotting phase velocities from the vibration modes of the beam-like specimens*

The purposes of computing and plotting the phase velocities of the beam-like specimens are to validate qualitatively the mechanical parameters (Young's modulus, Poisson ratio and density) and, consequently, the mode dispersion as predicted by the elastodynamic models from the dispersion curve. The phase velocities are first computed from the resonance

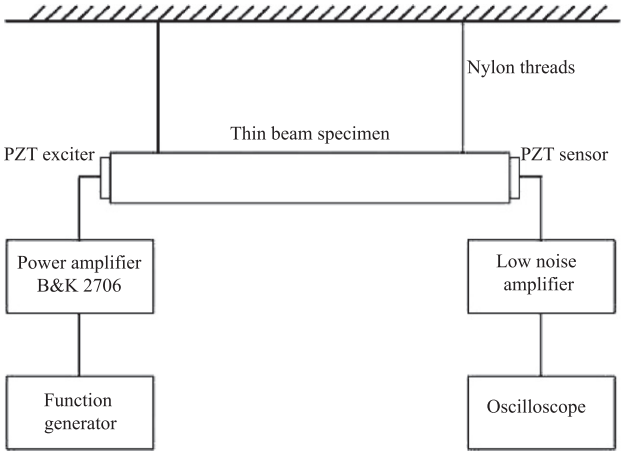


**Fig. 4.** The excitation and detection of longitudinal modes using PZT. The flexural modes are excited and detected by placing the transducers laterally.

frequencies $f^m_{\text{resonance}}$ and the length of the beams $L_{\text{beam}}$ using the simple relation:

$$v_{\text{phase}} = \frac{2L_{\text{beam}} f^m_{\text{resonance}}}{m}, \tag{13}$$

wherein $m$ is the mode number. The time taken for the wave induced by the exciter to reach the sensor (the two are placed at known positions) is then determined for each mode using the distance separating the two transducers, $L_{\text{exc-sens}}$. Herein $L_{\text{exc-sens}}=L_{\text{beam}}$. However, it should be noted that these simple computations are only valid for uniform, thin cross-section beams.

*7.2.3. Acquisition of induced transient wave response of thin beam-like specimens and visualization of wave dispersion using time–frequency representations*

A transient wave generated by a waveform function generator, Agilent 33250B, is induced in the specimen by the exciter PZT using the previous configuration. A steep voltage rise of the leading edge of a long positive rectangular pulse produced by the generator causes the PZT to deform and to induce a very short elastic wave pulse in the specimen. A second pulse is subsequently generated at the trailing edge of the rectangular pulse, but this is made to happen outside of the signal capture window. The response is measured using the PZT sensor. The pulse waveform on the receiver sensor is captured using an oscilloscope, Tektronix TDS 3032B. To obtain signals with higher signal-to-noise ratios, triggered averaging (512 temporal signals) is carried out. Bilinear time–frequency, Wigner–Ville distribution (WVD) [38] is used to analyze the transient signal and is plotted as a time–frequency representation (TFR). The WVD achieves better resolution in both the time and frequency domains, thus providing a critical advantage over standard Fourier analysis. TFR is more effective in localizing multiple, closely spaced modes in both time and frequency.

The validation consists in the comparison to known asymptotic values of the phase velocity of the fundamental longitudinal mode (L(0,1)) of a free isotropic bar whose static limit (called the bar velocity is $v_{\text{bar}} = \sqrt{E_b/\rho_b}$). The Rayleigh velocity for the propagation of a surface wave on the surface of a semi-infinite half-space is used for the validation at the high frequency limit of the fundamental flexural (also known as F(1,1)) and the L(0,1) modes. At the short wave length limit (high frequency), the Rayleigh beam theory predicts a wave velocity that approaches the surface wave velocity [39]. This velocity is given by $v_{\text{ray}} = \sqrt{N/\rho_b}((0.87+1.12\nu_b)/(1.0+\nu_b))$.

The two asymptotes on the time–frequency plane corresponding to the arrival times of waves that would have traveled in the beam with the two velocities are shown on the same plot as the TFR. The distance traveled is $L_{\text{exc-sens}}$.

The phase velocities are then constructed from resonance frequencies as explained in Section 7.2.2. The optimized values of the parameters obtained from the BJKCA model with the transmitted USW are employed in both of the elastodynamic models to compute the resonance frequencies. The resulting phase velocities are transcribed onto the same plot as the TFR of the measured transient signal.

The TFR indicates the arrival times of propagating vibrational modes captured by the sensor at the opposite end of the beam. It also allows the visualization of the temporal location of the spectral components, consequently mode dispersion.

The Time–Frequency Toolbox for Matlab developed in [40] was employed for the TFR computations in this study.

Other methods that can be employed for recovering the shear modulus and Poisson ratio include using phase velocities of guided acoustic modes from the displacement measured on a soft thick poroelastic plate excited by a mechanical shaker [41] and recovering the damping and shear modulus of the foam using Rayleigh waves detected acoustically over a thin porous layer (reticulated plastic foam) and the Biot theory [41,42]. These methods, however, require very large porous samples.

**Table 2**
Parameters of the BJKCA model with air as saturating fluid.

| Parameter | Symbol |
|---|---|
| Density of the pore fluid | $\rho_f$ |
| Density of porous skeletal frame | $\rho_b$ |
| Young's modulus of the porous skeletal frame | $E_b$ |
| Poisson ratio of the porous skeletal frame | $\nu_b$ |
| Fluid bulk modulus | $K_f$ |
| Porosity | $\phi$ |
| Tortuosity | $\alpha_\infty$ |
| Viscosity of pore fluid | $\eta$ |
| Viscous characteristic length | $\Lambda$ |
| Thermal characteristic length | $\Lambda'$ |

## 8. Results

In this section, results of the inversions are presented by plotting the cost/objective function obtained by the method described at the end of Section 3.

The elastic moduli of YPUF and melamine foam panels are recovered by solving the inverse vibration spectroscopy problem of their beam specimens. The cost functions for the IVS are not shown as the problem is well posed, the minima were found to be unique (single global minimum) [37].

### 8.1. Green polyurethane foam (GPUF)

The computed cost functions for the poroelastic parameters, obtained from the measured transmitted wave (at 50 and 100 kHz transducer as emitters and a microphone for reception) using the BJKCA model, are shown in Fig. 5. The retrieved parameters, which are solutions of the inverse problem, are read from these curves. The recovered density of 30 kg/m$^3$ is in a fair agreement with the measured one (32 kg/m$^3$). The transmitted signal is then reconstructed using the BJKCA model with these retrieved values and the measured incident signal as input. A particular aspect of the cost function is its sharpness in the neighborhood of one of its minima. It increases with the central transducer frequency. The CF of the 100 kHz is sharper than the 50 kHz one. The number of minima also increases with frequency. This sharpness allows a faster convergence and a more precise solution of the inverse problem [37]. The comparison between the transmitted (measured and reconstructed using retrieved parameters) signals is shown in Fig. 6. The excellent agreement between the two shows that the poroelastic parameters have been well-reconstructed.

### 8.2. Yellow polyurethane foam (YPUF)

The cost functions computed from transmitted data obtained using three different transducers (centered at 50, 100 and 200 kHz) insonifying a YPUF panel are shown in Fig. 7a–f. The measured density ($\rho_b$) of 27.8 kg/m$^3$ was in excellent agreement with the recovered one of 28 kg/m$^3$ (Fig. 7f). It is also within the range of those reported in [5,31]. There was equally a good agreement between YM and Poisson ratio recovered using BJKCA with transmitted USW (205 kPa, 0.47) and vibration spectroscopy (210 kPa, 0.47) (difference $\leq 2.4$ percent). The comparison between the measured and reconstructed transmitted signals is shown in Fig. 8. There is equally a good agreement between the two.

### 8.3. Melamine foam specimen

The recovered mechanical parameters for the melamine panel are $E_b$=180 kPa, $\nu_b = 0.46$ and $\rho_b = 8.0\,\mathrm{kg/m^3}$. The density $\rho_b$ of the melamine foam was determined from the weight on a balance and volume measurements (the density given by BASF for Basotec foam is 8.35 kg/m$^3$).

The retrieved $\Lambda$ was 107 μm. The average length of the foam ligament (taken between two ligaments, $l \approx 49\,\mu\mathrm{m}$), the edge breadth ($b_e \approx 4.15\,\mu\mathrm{m}$) and the radius of the cross-section ($r_{cs} \approx 2.8\,\mu\mathrm{m}$) are measured on the micrographs (Fig. 2a). Using these parameters and the formula for porosity given in [7]:

$$\phi = 1 - \left( \frac{b_e^2\sqrt{3}}{2} + 6\left[ l^2 \arcsin\left(\frac{b_e}{2l}\right) - \frac{b_e l}{2}\sqrt{1 - \frac{b_e^2}{4r_{cs}^2}} \right] \right) \Big/ \frac{3\sqrt{3}l^2}{2} \tag{14}$$

a porosity of 0.97 is obtained. This is in good agreement with the recovered one from transmitted USW data of 0.96.

The elastic moduli pair (Young's modulus, Poisson ratio) recovered by solving the inverse vibration spectroscopy problem for melamine are (178 kPa, 0.44). Poisson ratio is compared with the one established from a formulation for low density foam, function of relative density $\phi_s = \rho_b/\rho_s$. The formulation is from a constitutive model of the nonlinear elastic

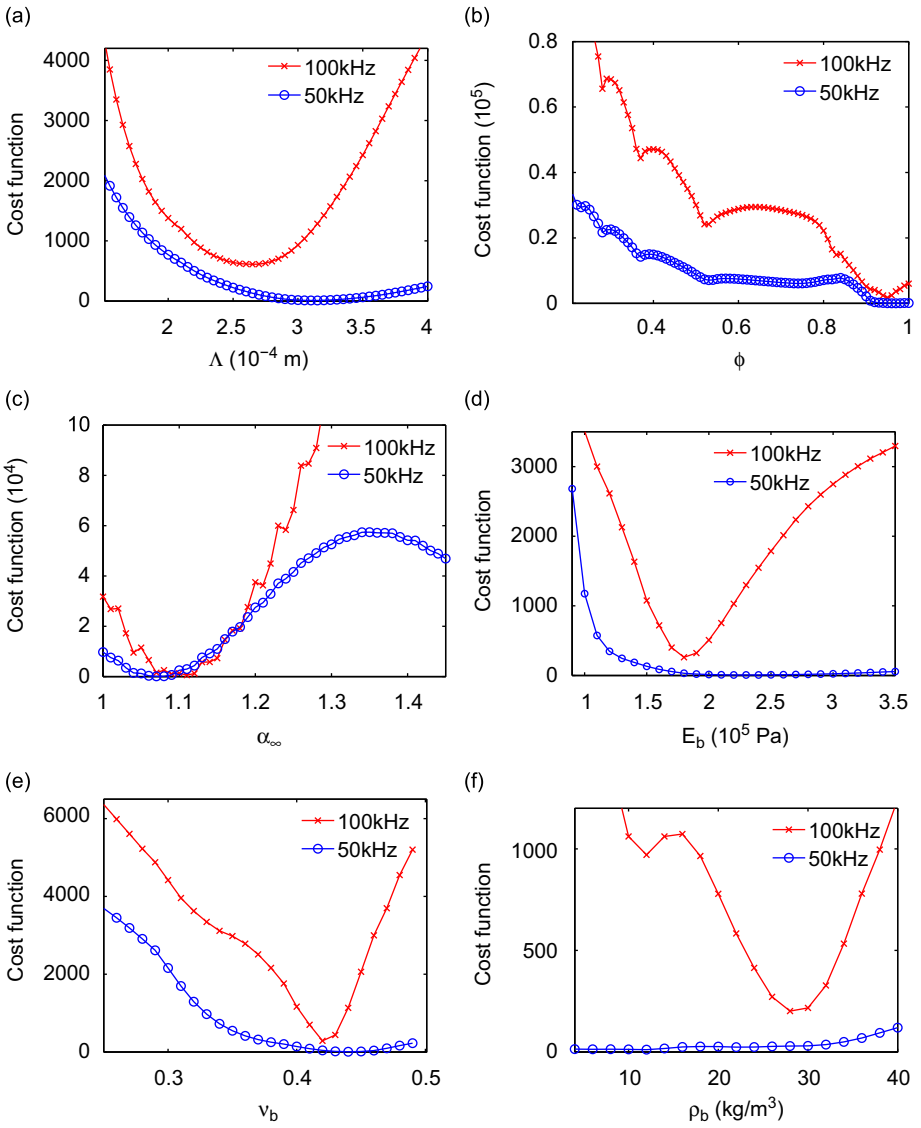


**Fig. 5.** The cost functions for the acoustic parameters of a 1.0 cm thick green polyurethane panel (using 50 and 100 kHz probes). The poroelastic parameters read from the common minima of the CF curves. In (a–c) are shown the acoustic parameters ($\Lambda$, $\phi$, $\alpha$). In (d–f), the mechanical parameters ($E_b$, $\nu_b$, $\rho_b$).

behavior of an isotropic low-density 3D open-cell using micromechanical analysis of an idealized tetrahedral unit cell [43],

$$\nu_b = 0.5 - 2.29\phi_s + 8.73\phi_s^2. \tag{15}$$

A $\nu_b$ of 0.43 is retrieved using the porosity $\phi$ (since $\phi_s = 1-\phi$) previously recovered from micromechanical analysis of the melamine foam. Jaouen et al. [44] reported a value of around 0.45 obtained from uniaxial compression load testing. Both values are in good agreement with the ones recovered employing the BJKCA and IVS methods.

The density used in the IVS scheme is from Table 1 which is also in good agreement (difference $\leq 2$ percent) with the one from BJKCA with transmitted USW.

### 8.4. Summary of the recovered parameters

The recovered poroelastic parameters using measured, incident and transmitted ultrasonic waves and the BJKCA model, are summarized in Table 3. The parameters retrieved using the model of equivalent fluid [13] and real data employing 200 kHz transducers are also shown for the sake of comparison. The values are in excellent agreement. The recovered densities agree well with the measured ones shown in Table 1. Densities of foams vary with the porosity [32]. YM depends on cell-wall bending, cell-wall axial deformation and fluid flow between the cells.

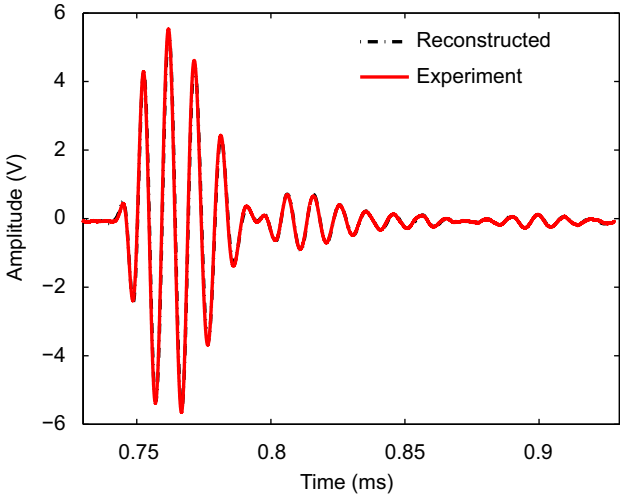


**Fig. 6.** The reconstructed transmitted signal for the green polyurethane foam (GPUF) panel using a 100 kHz ultrasonic air transducer and microphone. The amplitude measured in volt (V) is proportional to the acoustic pressure.

*8.4.1. Validation of tortuosity $\alpha_\infty$ of the open-cell foam specimens*

The asymptotes of the phase velocities for the three open pore foams are shown in Fig. 9. The measured velocity of sound $c_0$ in air was 342 m/s at 20 °C. The asymptotic phase velocities for melamine, GPUF, YPUF are 339, 329, 311 m/s and the resulting tortuosities are 1.019, 1.08 and 1.21, respectively. These are in excellent agreement with those from the BJKCA with transmitted USW. Since the asymptote of the phase velocity is beyond 200 kHz for the YPUF, three transducers at different central frequencies (50, 100 and 200 kHz) were used to retrieve its parameters to verify that they were approximately independent of transducer frequencies employed herein. Indeed these values are very close (Fig. 7) but vary with the frequency — difference $\leq 2.5$ percent. These are within the range of different measurement errors.

*8.5. Phase diagrams*

The configuration for the generation of transient flexural and compressional waves, as depicted in the setup in Fig. 4, was employed. The temporal signal, representing the transient waves (longitudinal excitation) propagating in the melamine beam is shown in the upper panel of Fig. 10. Ridges extracted from the computed TFR using the reassigned Pseudo Wigner–Ville distribution (RPWV) [38] of the measured transient response are shown in the background of the plot in the lower panel.

The superposition of the asymptotes of mode L(0,1) (the fundamental mode, i.e., low frequency) with the ridges converging to the bar velocity time line $t_{v_{\text{bar}}}$ on the time–frequency curves confirms qualitatively the validity of the parameters ($E_b$, $\rho_b$) recovered from the BJKCA with transmitted USW. For the F(1,1) mode, the moduli ($E_b$ and $\nu_b$) and density $\rho_b$ are used to calculate the time line $t_{v_{\text{ray}}}$.

The computed phase velocities are transcribed onto the same curve as the TFR (lower panel of Fig. 10) using the distance $L_{\text{exc-sens}}$. It is remarked that the computed 3D FEM L(0,1) and the Timoshenko beam model F(1,1) modes follow similar trajectories as the ridges consequently indicating similar dispersion mechanisms in the beam as integrated in the models.

## 9. Discussion and conclusion

This study highlights that employing an ultrasonic incident wave initially propagating in the air medium is able to carry some information on the elastic properties of the frame. Usually, at 50 kHz or higher frequencies, the solid phase is considered as immobile when solicited from air generated waves and the approximation of a rigid frame is often assumed, i.e., that the waves inside the porous material propagate only inside the fluid phase. Implicitly, if the waves carry some information on the elastic properties of the solid phase, this means that the waves are also propagating in the solid part and that the approximation of the rigid frame is valid only as a first approximation. This is the first time the BJKCA model is used to recover the poroelastic material parameters of soft plastic open-cell foams from measurements of transmitted USW in air.

The inconvenience of using reflected waves to characterize high porosity cellular materials is the poor signal to noise ratio (SNR) consequently penalizing the precision of the measurements. This is an advantage to the BJKCA model that requires only the measured incident and transmitted USW for the characterization of the porous medium (recall that the

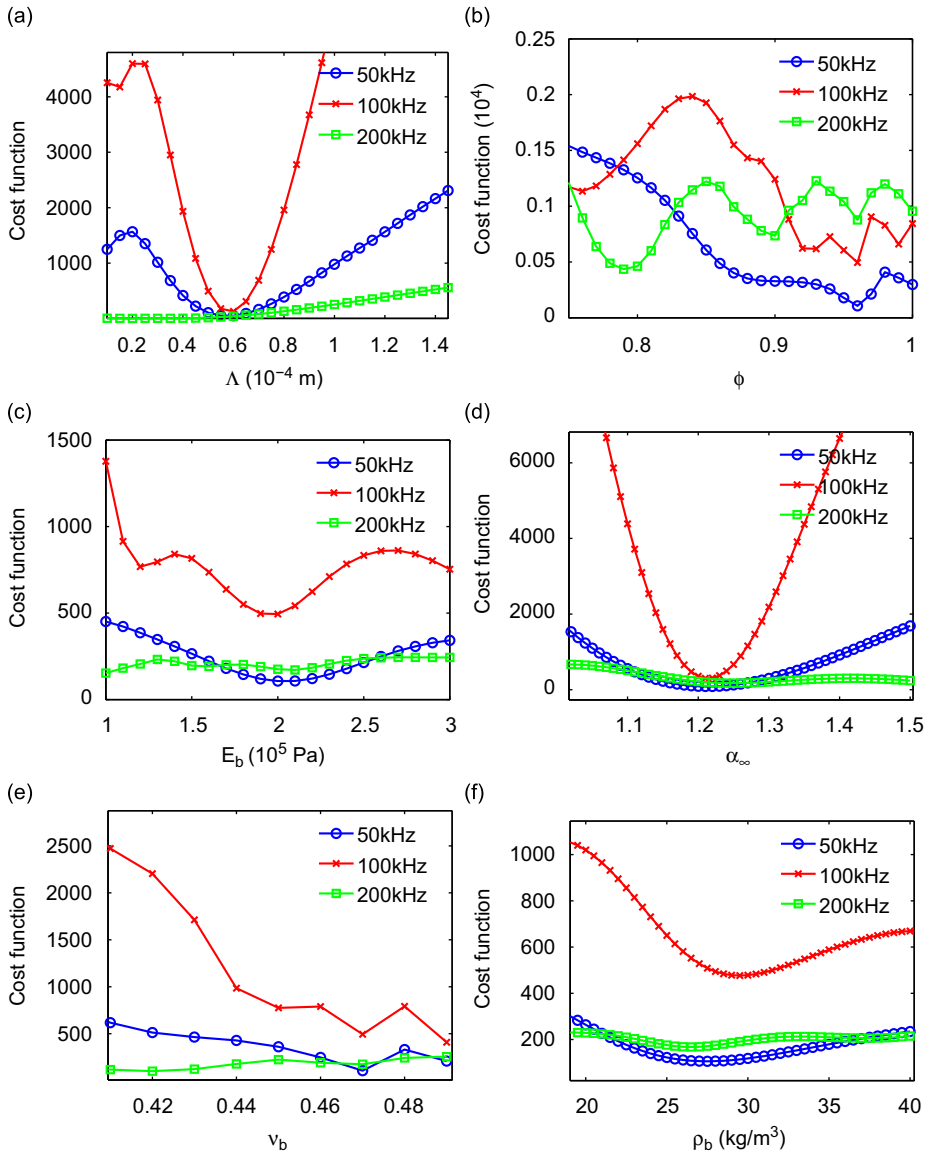


**Fig. 7.** The cost functions obtained by varying the poroelastic parameters using the incident and transmitted waves with the BJKCA model of a 1.0 cm thick, yellow polyurethane foam (YPUF) panel insonified by transducers at three center frequencies of 50, 100 and 200 kHz.

model of equivalent fluid requires the incident, reflected and transmitted waves). However, a low SNR of the transmitted wave also occurs in cases of high resistivity or very thick foams.

While time–frequency representations are often difficult to interpret, we have shown in the present study, using 3D Finite element analysis and 1D Timoshenko beam model equation solved by a finite difference method, that the trajectories of the TFR of the transient response represent the different propagating modes in the specimen with the L(0,1) mode the most visible. Comparison to known asymptotic values such as the bar and Rayleigh velocities provided extra criteria for validation of the recovered parameters. These asymptotes are well marked on the TFR plots consequently eliminating ambiguities in the determination of these velocities. The superposition of the trajectories of the modes computed from the elastodynamic models with those from the transient wave propagation experiment as visualized on the TFR plot indicates that the dispersion mechanisms in the beam specimens are those predicted by the models (Poisson effect, shear and rotary inertia).

A non-ambiguous technique for recovering the poroelastic parameters of cellular panels from cost functions that exhibit several minima has been developed. They were constructed using the BJKCA model as estimator and real data obtained from measured incident and transmitted ultrasound waves using several transducers with different central frequencies. The skeletal elastic parameters were verified by solving the inverse problem of retrieval of the elastic moduli using

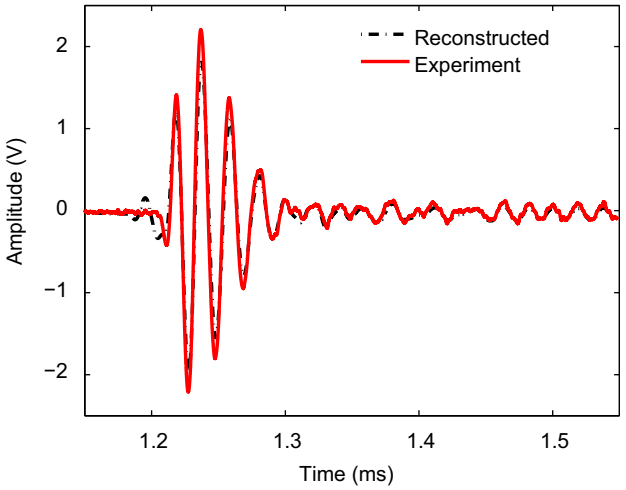


**Fig. 8.** The reconstructed transmitted signal using recovered values of the poroelastic parameters using BJKCA for the yellow polyurethane foam (YPUF) panel. The 100 kHz ultrasonic air transducer and microphone are employed.

**Table 3**
Summary of the poroelastic parameters recovered from the measured incident and transmitted USW using the BJKCA theory for open-cell foams and vibration spectroscopy (VS) data on beam sub-specimens.

| Foam | $\phi$ | | $\alpha_\infty$ | | $\Lambda$ (μm) | | $E_b$ (MPa) | | $\nu_b$ | | $\rho_b$ (kg m$^{-3}$) |
|---|---|---|---|---|---|---|---|---|---|---|---|
| | BJKCA | EFM | BJKCA | EFM | BJKCA | EFM | BJKCA | VS | BJKCA | VS | BJKCA |
| Melamine | 0.96 | 0.97 | 1.02 | 1.015 | 107 | 99 | 0.18 | 0.178 | 0.46 | 0.44 | 8.0 |
| GPUF | 0.95 | 0.96 | 1.07 | 1.08 | 265 | 252 | 0.18 | – | 0.42 | – | 30.0 |
| YPUF | 0.96 | | 1.21 | | 60 | | 0.205 | 0.210 | 0.47 | 0.465 | 28 |

Values recovered using the model of equivalent fluid (MEF) and reflection and transmission data [13], obtained with USW transducers with center frequencies at 200 kHz, are also listed. Herein $\Lambda' = 3\Lambda$.

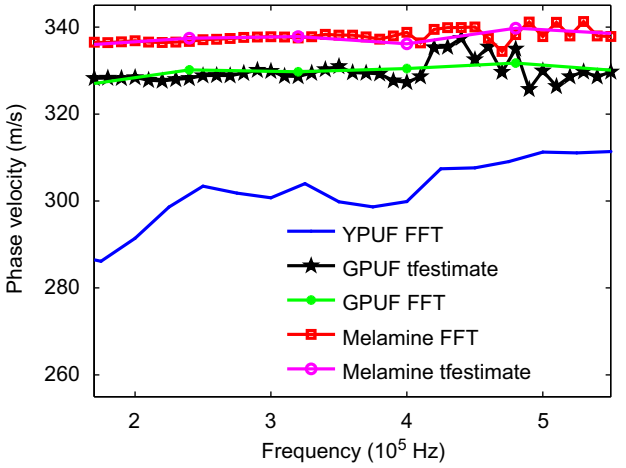


**Fig. 9.** Phase velocities for the melamine, YPUF and GPUF panels, calculated from the phase difference between the transmitted and incident waves using two different methods. The transfer function (Matlab [46] *tftestimate* function) and Fourier transform methods with phase unwrapping are employed. Two 200 kHz air coupled transducers (exciter and receiver) are employed.

vibration spectroscopy data measured on beam-like sub-specimens of the panels and a macroscopic 3D equivalent solid elastodynamic finite element model as estimator. Since the porous media are saturated with a light fluid (air), the recovered mechanical parameters (in the measurement frequency band) pertain to those of the skeleton. The mechanical moduli retrieved from the transmitted USW with the BJKCA model and those recovered from vibration spectroscopy with the elastodynamic model were found to be in excellent agreement.

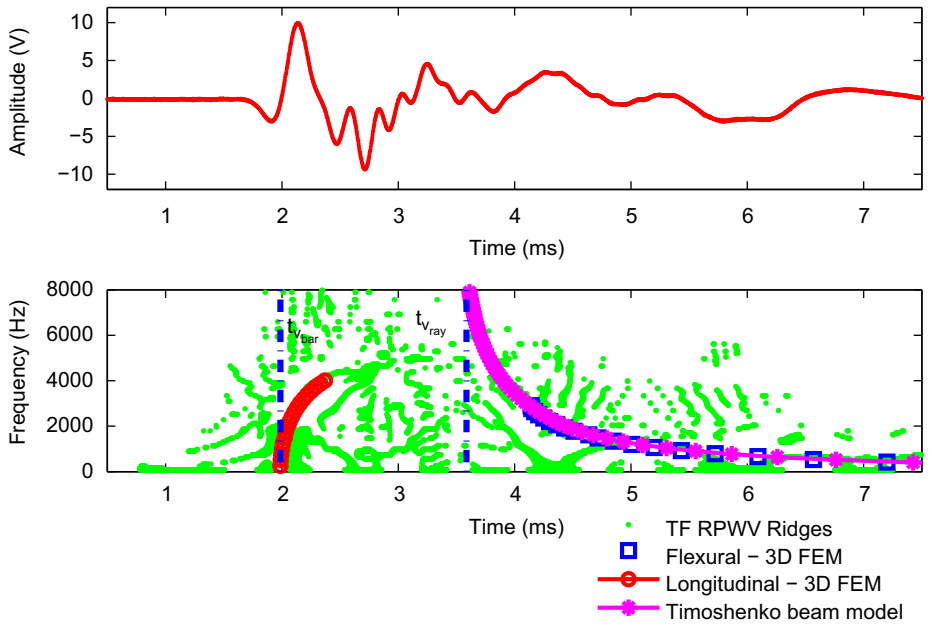


**Fig. 10.** In the upper panel, the measured transient response of the melamine foam using the configuration for the generation of flexural waves. In the lower panel, the corresponding computed ridge representation of the time–frequency decomposition (RPWV). Represented are also the theoretical dispersion curves calculated from the resonance frequencies computed using the 3D FEM modal analysis and the Timoshenko beam model.

Validation of the acoustic parameters was made using the MEF (the reference model for the acoustic characterization of open pore, soft plastic foams using USW data [13]). The results which were in excellent agreement show that the MEF (the foam skeleton is considered rigid and motionless in the absence of mechanical excitation) is an appropriate approximate model. However, the BJKCA model provides both the microstructural acoustic parameters ($\phi$, $\Lambda$, $\Lambda'=3\Lambda$, $\alpha_\infty$) and the mechanical parameters of the skeleton ($E_b$, $\nu_b$, $\rho_b$). In the low frequency regime where the frame can no longer be considered motionless, the BJKCA model should be employed.

A good agreement was also found between the retrieved $\alpha_\infty$ for open-cell foams using the measured asymptotic phase velocities of the panels with a 200 kHz transducer.

Images acquired by a scanning electron microscope provided an idea of the pore geometry and an indication of size. The acoustic method developed herein can be used for the validation of formulae developed for the calculation of parameters of cellular materials based on optical or electron microscopy measurements of geometric microstructural dimensions (e.g. porosity from ligament dimensions).

The plethora of foam types resulting from the diversity and constant evolution of their applications and foaming techniques makes the obtention of reliable tabulated data of the acoustic and mechanical characteristics difficult. This justifies the development of efficient and more reliable methods for recovering these parameters.

## Acknowledgements

The authors are thankful to Alain Busso for improving the ultrasonic test rig and machining the beam specimens used in this study. We are indebted to Alain Bernadac of Institut de Biologie Structurale et Microbiologie of GLM for allowing us access to the cellular Biology observation platform and especially the imaging microscopes. The authors are also grateful to the reviewers for their useful comments that have enabled the improvement of the manuscript quality.

## Appendix A. Experimental determination of tortuosity using transmitted USW

The approximation of the complex wavenumber $\mathcal{K}$ at high frequencies for a rigid frame porous material saturated by air is given in [45]

$$\mathcal{K}=\frac{\omega}{c_0}\sqrt{\alpha_\infty}\left(1+(1-\mathrm{j})\frac{\delta}{2}\left(\frac{1}{\Lambda}+\frac{\gamma-1}{\sqrt{P_r}\Lambda'}\right)\right), \tag{A.1}$$

where $c_0$ is the speed of sound in air and $\omega$ the angular frequency. At sufficiently high frequencies the viscous skin depth $\delta$ tends to zero and the phase velocity is asymptotically $c(\omega)\approx c_0/\sqrt{\alpha_\infty}$, thus providing a method for measuring $\alpha_\infty$.

The incident (in the absence of the porous panel sample) and the transmitted (in the presence of sample) waves at normal incidence are acquired. The phase difference between the two signals is computed using the *tfestimate* function in [46] which estimates the transfer function using Welch's averaged periodogram method [47]. The input and output of the system are the incident and transmitted signals, respectively. For foams with high tortuosity, the transmitted signal is very attenuated consequently the phase recovered is erroneous. In this case the phase difference between the two signals is calculated from the phases of their fast Fourier transforms (FFT). All the other phase differences have been computed using the two methods and the tortuosities obtained are in good agreement with those from the transmitted USW and BJKCA inverse method.

The phase velocity is computed from the expression

$$c(\omega)=\frac{Lc_0}{L+c_0\Delta t}, \tag{A.2}$$

where $\Delta t$ is the time lag between the incident and the transmitted signals and is calculated from the phase $\theta(\omega)$ of the transfer function, $\Delta t=\theta(\omega)/\omega$.

## Appendix B. Vibration spectroscopy — elastodynamic model

The body vibrates in response to the excitation and this phenomenon is described by the classical equations of the elastodynamics of continuous elastic media. Dissipation in the body, which can be accounted for by the introduction of Rayleigh damping [37], is neglected because only the resonance frequencies are of interest here.

The integral version of the governing partial differential equations (PDEs), which takes the form of the principle of virtual work, is discretized [48]. The eigenvalue problem for the natural modes takes the form

$$(\lambda_{eig}^2\mathbb{M}+\mathbb{K})\Phi=0, \tag{B.1}$$

with $\mathbb{M}$, $\mathbb{K}$ the mass and stiffness matrices, respectively, $\lambda_{eig}$ the eigenvalue and $\Phi$ the eigenvector (i.e., the vibration mode).

## Appendix C. Solving the Timoshenko beam model eigenvalue problem using finite difference method

Assuming a time-harmonic solution of the form $v(x,t)=v(x,\omega)\exp[\mathrm{j}(\Upsilon x-\omega t)]$, where $v(x,t)$ is the lateral displacement, $\Upsilon$ the wavenumber, the Timoshenko beam equation written as a single partial differential equation of the fourth order is

$$\frac{EI}{\rho A}\frac{\partial^4 v(x)}{\partial x^4}+\frac{\omega^2 I}{A}\left(1+\frac{E}{G\kappa}\right)\frac{\partial^2 v(x)}{\partial x^2}-\omega^2 v(x)+\frac{\omega^4\rho I}{GA\kappa}v(x)=0. \tag{C.1}$$

where $E$ is Young's, $G=E/2(1+\nu)$ the shear modulus, $\rho$ the density, $I$ the cross-sectional area moment of inertia, and $A$ the cross-sectional area of the beam. The values of the shear correction factor, $\kappa$ for simple geometrical cross-sections have been calculated by several authors [49–52]. Hutchinson's coefficients [52] were used here. An approximate numerical solution of this complex problem is obtained by the finite difference method (FDM). The derivatives are replaced by their appropriate fourth-order central-difference approximations. Consequently the eigenvalue problem which is solved to obtain the natural frequencies of the beam is [53]

$$\begin{aligned}&(-\alpha_T v_{i-3}+12\alpha_T v_{i-2}-39\alpha_T v_{i-4}+56\alpha_T v_i-39\alpha_T v_{i+1}-\alpha_T v_{i+3})\\&+\omega^2(-\beta_T v_{i-2}+16\beta_T v_{i-1}-(30\beta_T+1)v_i+16\beta_T v_{i+1}-\beta_T v_{i+2})+\omega^4\gamma_T v_i\approx 0\end{aligned} \tag{C.2}$$

with $i=0,1,\ldots,\alpha_T=(EI/\rho A)(1/6\hbar^4)$, $\beta_T=(I/A)(1+E/G\kappa)(1/12\hbar^2)$ and $\gamma_T=(\rho I/GA\kappa)$. If $n$ is the number of segments on the length of the beam then $\hbar=L_{\mathrm{beam}}/n$.

The boundary conditions (BC) corresponding to the stress-free beam are $\partial^2 v/\partial x^2=0$ and $\partial^3 v/\partial x^3=0$ at $x$=0 and at $x$=$L_{\mathrm{beam}}$.

The introduction of BC (at $i$=0 and $i$=$n$) and employing the lower-order FDM relations, the fictive points are found to be

$$\begin{aligned}&v_{-1}=2v_0-v_1,\quad v_{-2}=4(v_0-v_1)+v_2,\quad v_{-3}=6(v_0-v_1)+v_3,\\&v_{n+1}=2v_n-v_{n-1},\quad v_{n+2}=4(v_n-v_{n-1})+v_{n-2},\quad v_{n+3}=6(v_n-v_{n-1})+v_{n-3}.\end{aligned} \tag{C.3}$$

Eq. (C.2) is put into matrix form:

$$\mathbf{Cv}+\omega^2\mathbf{Bv}+\omega^4\mathbf{Av}=\mathbf{0}, \tag{C.4}$$

whereby $\mathbf{0}$ is a matrix of zeros. The matrix calculation entry for each position $i$ on the beam is given in Table 4.

Let $\Omega_T=\omega^2$, Eq. (C.4) becomes

$$\mathbf{C}+\Omega_T\mathbf{B}+\Omega_T^2\mathbf{A}=\mathbf{0}, \tag{C.5}$$

**Table 4**
The matrix table for the stress-free Timoshenko beam showing the equations of the points along the axis at positions *i*.

| *i* | Equation |
|---|---|
| 0 | $20\alpha_T v_0-42\alpha_T v_1+24\alpha_T v_2-2\alpha_T v_3+\omega^2(-(2\beta_T+1)v_0+4\beta_T v_1-2\beta_T v_2)+\omega^4\gamma_T v_0$ |
| 1 | $-19\alpha_T v_0+48\alpha_T v_1-40\alpha_T v_2+12\alpha_T v_3-\alpha_T v_4+\omega^2(14\beta_T v_0-(29\beta_T+1)v_1+16\beta_T v_2-\beta_T v_3)+\omega^4\gamma_T v_1$ |
| 2 | $10\alpha_T v_0-38\alpha_T v_1+56\alpha_T v_2-39\alpha_T v_3+12\alpha_T v_4-\alpha_T v_5\omega^2(-\beta_T v_0+16\beta_T v_1-(30\beta_T+1)v_2+16\beta_T v_3-\beta_T v_4)+\omega^4\gamma_T v_2$ |
| 3 to $n-3$ | $-\alpha_T v_{n-3}+12\alpha_T v_{n-2}-39\alpha_T v_{n-1}+56\alpha_T v_n-39\alpha_T v_{n+1}+12\alpha_T v_{n+2}$ $-\alpha_T v_{n+3}+\omega^2(-\beta_T v_{n-2}+16\beta_T v_{n-1}-(30\beta_T+1)v_n+16\beta_T v_{n+1}-\beta_T v_{n+2})+\omega^4\gamma_T v_n$ |
| $n-2$ | $-\alpha_T v_{n-5}+12\alpha_T v_{n-4}-39\alpha_T v_{n-3}+56\alpha_T v_{n-2}-38\alpha_T v_{n-1}+10\alpha_T v_n\omega^2(-\beta_T v_{n-4}$ $+16\beta_T v_{n-3}-(30\beta_T+1)v_{n-2}+16\beta_T v_{n-1}-\beta_T v_n)+\omega^4\gamma_T v_{n-2}$ |
| $n-1$ | $-\alpha_T v_{n-4}+12\alpha_T v_{n-3}-40\alpha_T v_{n-2}+48\alpha_T v_{n-1}-19\alpha_T v_n+\omega^2(-\beta_T v_{n-3}+16\beta_T v_{n-2}-(29\beta_T+1)v_{n-1}+14\beta_T v_n)+\omega^4\gamma_T v_{n-1}$ |
| $n$ | $-2\alpha_T v_{n-3}+24\alpha_T v_{n-2}-42\alpha_T v_{n-1}+20\alpha_T v_n+\omega^2(-2\beta_T v_{n-2}+4\beta_T v_{n-1}-(2\beta_T+1)v_n)+\omega^4\gamma_T v_n$ |

whose solutions are

$$\Omega_T\mathbf{I}=\frac{-\mathbf{B}\pm\sqrt{\mathbf{B}^2-4\mathbf{AC}}}{2}\mathbf{A}^{-1}, \tag{C.6}$$

where **I** the identity matrix. In Eq. (C.6), the following matrix is computed:

$$\mathbf{X}=\sqrt{\mathbf{BB}-4\mathbf{AC}}\coloneqq\mathbf{M}^{1/2}. \tag{C.7}$$

If **X** is the square root of the principal matrix **M**, then **XX=M**. Which means, **X**, is a unique root for which the real part of each eigenvalue is positive. If all the eigenvalues of **M** are negative, then the root is complex valued. If **M** is singular, then a root does not exist. The solutions for $\Omega_T$ are obtained from

$$\det(\Omega_T\mathbf{I}-\tfrac{1}{2}\mathbf{X}\mathbf{A}^{-1})=0, \tag{C.8}$$

where det stands for determinant. The eigenvalues are complex in this case:

$$\Omega_{T_k}=\varpi_k+\mathrm{j}\nu_k, \tag{C.9}$$

where $\nu_k$ is the damping factor and $\varpi_k$ the natural frequency of the mode ($k$).

The two solutions of Eq. (C.6) correspond to the two flexural wave modes propagating with different velocities. The slower mode is the most visible in the time frequency curves (lower frequencies are consequently less attenuated) while the faster (higher frequency) is more attenuated.

## Appendix D. Solving the inverse vibration spectroscopy

Recall that in order to compute the resonance frequencies, the eigenvalue problem for the natural modes must be solved employing the discretized form of the dynamic analysis equation given by Eq. (B.1) found in Appendix B.

The problem is solved iteratively by minimizing the cost function $\Im$ (which is a measure of the discrepancy between the model and experimental outputs):

$$\Im(E_b,\nu_b)=\sum_{p=1}^{m}\{f^p_{\text{experiment}}-f^p_{\text{model}}(E_b,\rho_b,\nu_b)\}^2, \tag{D.1}$$

with $f^p_{\text{experiment}}$ the target resonance frequency obtained by experiment, $p=1,2\ldots$ the mode number, $m$ the number of modes here $m=2$ for the beam and $f^p_{\text{model}}$ the natural frequency furnished by the model for the current trial value of $E_b$ and $\nu_b$. The density is taken from data obtained from the previous inverse problem (confirmed by calculating the volume and weighing the specimen). The minimization is carried out using the Levenberg–Marquardt algorithm (implemented in the *lmdif* routine from *Minpack*, conceived at the Argonne National Laboratory). The inverse problem of the retrieval of $E_b$ and $\nu_b$ appears to be well-posed, that is, there exist a unique solution for the sought-for parameters [37].

## References

[1] M. Ridha, V.P.W. Shim, Microstructural and tensile mechanical properties of anisotropic rigid polyurethane foam, *Experimental Mechanics* 49 (2008) 763–776.
[2] P. Onck, J.-F. Ganghoffer (Eds.), Special section: mechanical behavior of cellular solids, *Journal of Material Science* 40 (2005) 5791–6053.
[3] L. Gong, S. Kyriakides, W.-Y. Jang, Compressive response of open-cell foams. Part I: morphology and elastic properties, *International Journal of Solids and Structures* 45 (2005) 1355–1379.
[4] W.-Y. Jang, A.M. Kraynik, S. Kyriakides, On the microstructure of open-cell foams and its effect on elastic properties, *International Journal of Solids and Structures* 45 (2008) 1845–1875.
[5] N. Mills, The high strain mechanical response of the wet Kelvin model for open-cell foams, *International Journal of Solids and Structures* 44 (1) (2007) 51–65.

[6] N.J. Mills, The wet Kelvin model for air flow through open-cell polyuethane foams, *Journal of Materials Science* 40 (2005) 5851–5945.
[7] C. Perrot, F. Chevillotte, R. Panneton, Bottom-up approach for microstructure optimization of sound absorbing materials, *The Journal of the Acoustical Society of America* 124 (2) (2008) 940–948.
[8] J. Allard, *Propagation of Sound in Porous Media: Modeling Sound Absorbing Materials*, Elsevier Applied Science, 1993.
[9] B. Lagrain, L. Boeckx, E. Wilderjans, J. Delcour, W. Lauriks, Non-contact ultrasound characterization of bread crumb: application of the Biot–Allard model, *Food Research International* 39 (10) (2006) 1067–1075.
[10] A. Wirgin, Ill-posedness and accuracy in connection with the recovery of a single parameter from a single measurement, *Inverse Problems in Science and Engineering* 10 (2) (2002) 105–115.
[11] E. Ogam, A. Wirgin, Recovery of the location, size, orientation and shape of a rigid cylindrical body from simulated and experimental scattered acoustic field data, *Inverse Problems in Science and Engineering* 12 (4) (2004) 433–469.
[12] H.W. Engl, M. Hanke, A. Neubauer, *Regularization of Inverse Problems*, Kluwer, Dordrecht, 1996.
[13] Z. Fellah, F. Mitri, M. Fellah, E. Ogam, C. Depollier, Ultrasonic characterization of porous absorbing materials: inverse problem, *Journal of Sound and Vibration* 302 (4–5) (2007) 746–759.
[14] N. Sebaa, Z.E.A. Fellah, M. Fellah, E. Ogam, A. Wirgin, F.G. Mitri, C. Depollier, W. Lauriks, Ultrasonic characterization of human cancellous bone using the Biot theory: inverse problem, *The Journal of the Acoustical Society of America* 120 (4) (2006) 1816–1824.
[15] N. Atalla, F. Sgard, Modeling of perforated plates and screens using rigid frame porous models, *Journal of Sound and Vibration* 303 (1–2) (2007) 195–208.
[16] J.-P. Groby, E. Ogam, L.D. Ryck, N. Sebaa, W. Lauriks, Analytical method for the ultrasonic characterization of homogeneous rigid porous materials from transmitted and reflected coefficients, *The Journal of the Acoustical Society of America* 127 (2) (2010) 764–772.
[17] D.L. Johnson, J. Koplik, R. Dashen, Theory of dynamic permeability and tortuosity in fluid-saturated porous media, *Journal of Fluid Mechanics* 176 (1987) 379–402.
[18] N. Sebaa, Z.E.A. Fellah, M. Fellah, W. Lauriks, C. Depollier, Measuring flow resistivity of porous material via acoustic reflected waves, *Journal of Applied Physics* 98 (8) (2005) 084901.
[19] O. Umnova, K. Attenborough, H.-C. Shin, A. Cummings, Response of multiple rigid porous layers to high levels of continuous acoustic excitation, *The Journal of the Acoustical Society of America* 116 (2) (2004) 703–712.
[20] P. Leclaire, L. Kelders, W. Lauriks, C. Glorieux, J. Thoen, Determination of the viscous characteristic length in air-filled porous materials by ultrasonic attenuation measurements, *The Journal of the Acoustical Society of America* 99 (4) (1996) 1944–1948.
[21] S.M. Han, H. Benaroya, T. Wei, Dynamics of transversely vibrating beams using four engineering theories, *Journal of Sound and Vibration* 225 (5) (1999) 935–988.
[22] K.F. Graff, *Wave Motion in Elastic Solids*, Dover Publications, Inc, New York, 1991.
[23] M.A. Biot, D.G. Willis, The elastic coefficients of the theory of consolidation, *Journal of Applied Mechanics* 24 (1957) 594–601.
[24] Y. Champoux, J.-F. Allard, Dynamic tortuosity and bulk modulus in air-saturated porous media, *Journal of Applied Physics* 70 (1991) 1975–1979.
[25] A. Moussatov, C. Ayrault, B. Castagnède, Porous material characterization—ultrasonic method for estimation of tortuosity and characteristic length using a barometric chamber, *Ultrasonics* 39 (3) (2001) 195–202.
[26] Z.E.A. Fellah, J.Y. Chapelon, S. Berger, W. Lauriks, C. Depollier, Ultrasonic wave propagation in human cancellous bone: application of Biot theory, *The Journal of the Acoustical Society of America* 116 (1) (2004) 61–73.
[27] D.P. Bertsekas, *Nonlinear Programming*, second ed., Athena Scientific, 1999.
[28] P. Leclaire, L. Kelders, W. Lauriks, M. Melon, N. Brown, B. Castagnède, Determination of the viscous and thermal characteristic lengths of plastic foams by ultrasonic measurements in helium and air, *Journal of Applied Physics* 80 (4) (1996) 2009–2012.
[29] N. Kino, T. Ueno, Y. Suzuki, H. Makino, Investigation of non-acoustical parameters of compressed melamine foam materials, *Applied Acoustics* 70 (4) (2009) 595–604.
[30] S. Schneider, Numerical prediction of the quality of an anechoic chamber in the low frequency range, *Journal of Sound and Vibration* 320 (4–5) (2009) 990–1003.
[31] L.J. Gibson, M.F. Ashby, *Cellular Solids: Structure and Properties, Cambridge Solid State Science*, second ed., Cambridge University Press, 1997.
[32] L. Gong, S. Kyriakides, N. Triantafyllidis, On the stability of Kelvin cell foams under compressive loads, *Journal of the Mechanics and Physics of Solids* 53 (4) (2005) 771–794.
[33] N. Mills, Micromechanics of polymeric foams, *Proceedings of the Third Nordic Meeting on Materials and Mechanics*, Aalborg Denmark, 2000, pp. 45–76.
[34] M.A. Biot, Theory of propagation of elastic waves in a fluid-saturated porous solid. I. Low-frequency range, *The Journal of the Acoustical Society of America* 28 (2) (1956) 168–178.
[35] M.A. Biot, Theory of propagation of elastic waves in a fluid-saturated porous solid. II. Higher frequency range, *The Journal of the Acoustical Society of America* 28 (2) (1956) 179–191.
[36] M. Henry, M. Bruneau, C. Potel (Eds.), *Matériaux acoustique*, vol. 3, Lavoisier, Paris, France, 2006, pp. 157–183.
[37] E. Ogam, A. Wirgin, S. Schneider, Z. Fellah, Y. Xu, Recovery of elastic parameters of cellular materials by inversion of vibrational data, *Journal of Sound and Vibration* 313 (3–5) (2008) 525–543.
[38] F. Auger, P. Flandrin, Improving the readability of time–frequency and timescale representations by the reassignment method, *IEEE Transactions on Signal Processing* 43 (1995) 1068–1098.
[39] R.D. Mindlin, G. Herrmann, A one-dimensional theory of compressional waves in an elastic rod, in: *Proceedings of the 1st U.S. National Congress of Applied Mechanics*, ASME, New York1951, pp. 187–191.
[40] F. Auger, O. Lemoine, P. Gonçalves, P. Flandrin, Time–frequency toolbox, Developed with the support of the CNRS (France) and Rice University (USA) and is freely available on the WWW, 1997. URL: 〈http://tftb.nongnu.org/〉.
[41] L. Boeckx, P. Leclaire, P. Khurana, C. Glorieux, W. Lauriks, J.F. Allard, Investigation of the phase velocities of guided acoustic waves in soft porous layers, *The Journal of the Acoustical Society of America* 117 (2) (2005) 545–554.
[42] J.F. Allard, M. Henry, L. Boeckx, P. Leclaire, W. Lauriks, Acoustical measurement of the shear modulus for thin porous layers, *The Journal of the Acoustical Society of America* 117 (4) (2005) 1737–1743.
[43] W.E. Warren, A.M. Kraynik, The linear elastic properties of open-cell foams, *Journal of Applied Mechanics* 55 (2) (1988) 341–346.
[44] L. Jaouen, A. Renault, M. Deverge, Elastic and damping characterizations of acoustical porous materials: available experimental methods and applications to a melamine foam, *Applied Acoustics* 69 (12) (2008) 1129–1140.
[45] D. Lafarge, J.F. Allard, B. Brouard, C. Verhaegen, W. Lauriks, Characteristic dimensions and prediction at high frequencies of the surface impedance of porous layers, *The Journal of the Acoustical Society of America* 93 (5) (1993) 2474–2478.
[46] Matlab, *Matlab V7.0*, Mathworks, Inc, Natick, MA, 1999.
[47] P.D. Welch, The use of fast Fourier transform for the estimation of power spectra: a method based on time averaging over short, modified periodograms, *IEEE Transactions on Audio and Electroacoustics* AU-15 (1967) 70–73.
[48] T.J.R. Hughes, *Finite Element Method—Linear Static and Dynamic Finite Element Analysis*, Prentice-Hall, Englewood Cliffs, 2000.
[49] S. Timoshenko, On the correction for shear of the differential equation for transverse vibrations of prismatic bars, *Philosophical Magazine* 41 (1921) 744–746.
[50] S. Timoshenko, On the transverse vibrations of bars of uniform cross-section, *Philosophical Magazine* 43 (1922) 125–131.
[51] G.R. Cowper, The shear coefficient in Timoshenko's beam theory, *Journal of Applied Mechanics* 33 (1966) 335–340.
[52] J.R. Hutchinson, Shear coefficient for Timoshenko beam theory, *Journal of Applied Mechanics* 68 (2001) 87–92.
[53] E. Ogam, Caractérisation ultrasonore et vibroacoustique de la santé mécanique des os humains (Ultrasonic and vibroacoustic characterization of the mechanical health of human bones), PhD Thesis, Université de Provence (Aix-Marseille I), Marseille France, 2007. URL: 〈http://tel.archives-ouvertes.fr/tel-00349558/en/〉.